

AD-A054 896

COLD REGIONS RESEARCH AND ENGINEERING LAB HANOVER N H F/G 8/12
THE VISCOELASTIC DEFLECTION OF AN INFINITE FLOATING ICE PLATE S--ETC(U)
APR 78 S TAKAGI
CRREL-78-5

UNCLASSIFIED

NL

| OF |
AD
A054896



END
DATE
FILMED
7-78
DDC

AD A 05 4896

CRREL REPORT 78-5

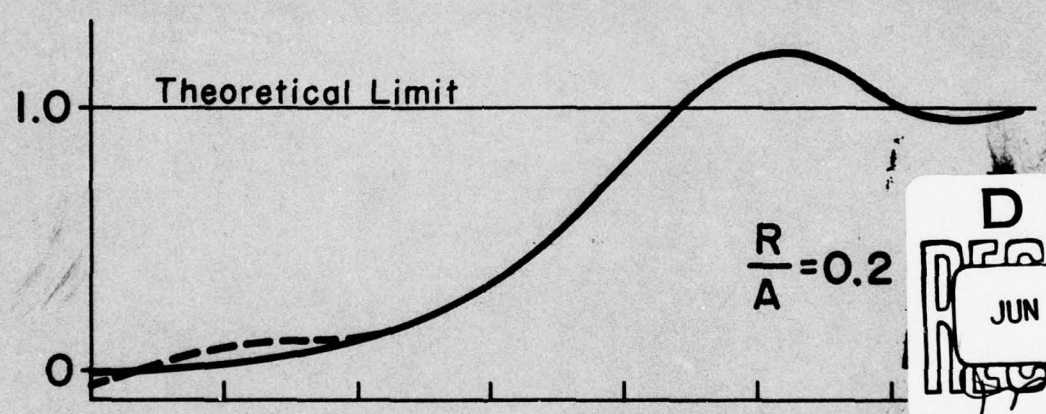
FOR FURTHER TRAN

16

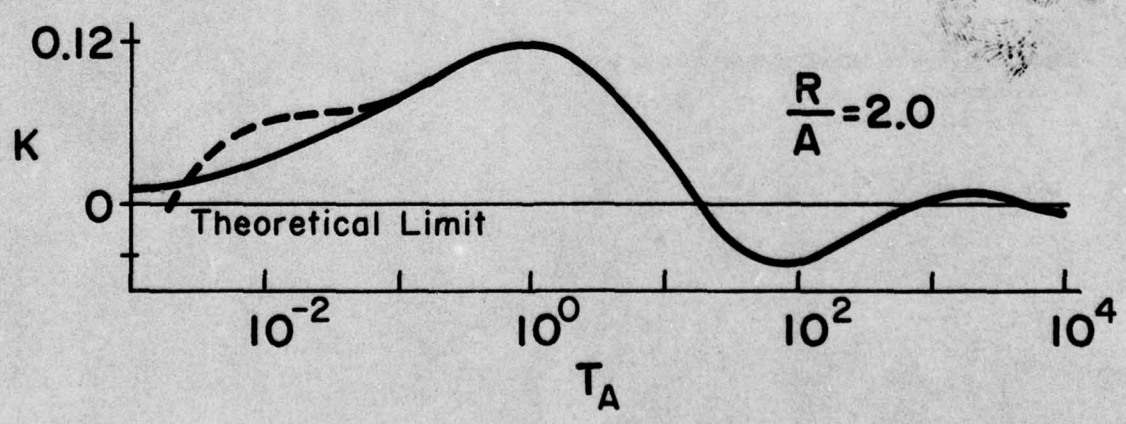


The viscoelastic deflection of an infinite floating ice plate subjected to a circular load

DDC FILE COPY
K



DDC
JUN 9 1978
E



DISTRIBUTION STATEMENT A
Approved for public release;
Distribution Unlimited

Cover: Graphs of asymptotic integral K in equation (6.4)

— Exact curve
---- Asymptotic curve

CRREL Report 78-5

9

6 The viscoelastic deflection of an infinite floating ice plate subjected to a circular load,

10 Shunsuke/Takagi

11 Apr 78

12 36 p.

14 CRREL-78-5

16 4A161102AT24

17 A1

DDC
JUN 9 1978
E

Prepared for
DIRECTORATE OF FACILITIES ENGINEERING
OFFICE, CHIEF OF ENGINEERS
By
CORPS OF ENGINEERS, U.S. ARMY
COLD REGIONS RESEARCH AND ENGINEERING LABORATORY
HANOVER, NEW HAMPSHIRE

Approved for public release, distribution unlimited.

037 100

mt

Unclassified

SECURITY CLASSIFICATION OF THIS PAGE (When Data Entered)

REPORT DOCUMENTATION PAGE		READ INSTRUCTIONS BEFORE COMPLETING FORM
1. REPORT NUMBER CRREL Report 78-5	2. GOVT ACCESSION NO.	3. RECIPIENT'S CATALOG NUMBER
4. TITLE (and Subtitle) THE VISCOELASTIC DEFLECTION OF AN INFINITE FLOATING ICE PLATE SUBJECTED TO A CIRCULAR LOAD		5. TYPE OF REPORT & PERIOD COVERED
		6. PERFORMING ORG. REPORT NUMBER
7. AUTHOR(s) Shunsuke Takagi		8. CONTRACT OR GRANT NUMBER(s)
		10. PROGRAM ELEMENT, PROJECT, TASK AREA & WORK UNIT NUMBERS DA Project 4A161102AT24 Task A1, Work Unit 001
9. PERFORMING ORGANIZATION NAME AND ADDRESS U.S. Army Cold Regions Research and Engineering Laboratory Hanover, New Hampshire 03755		12. REPORT DATE April 1978
		13. NUMBER OF PAGES 34
11. CONTROLLING OFFICE NAME AND ADDRESS Directorate of Facilities Engineering Office, Chief of Engineers Washington, D.C. 20314		15. SECURITY CLASS. (of this report)
		15a. DECLASSIFICATION/DOWNGRADING SCHEDULE
14. MONITORING AGENCY NAME & ADDRESS (if different from Controlling Office)		
16. DISTRIBUTION STATEMENT (of this Report) Approved for public release; distribution unlimited.		
17. DISTRIBUTION STATEMENT (of the abstract entered in Block 20, if different from Report)		
18. SUPPLEMENTARY NOTES		
19. KEY WORDS (Continue on reverse side if necessary and identify by block number) Bessel functions Ice plate Numerical integration Viscoelasticity		
20. ABSTRACT (Continue on reverse side if necessary and identify by block number) <p>We solved^{WAS SOLVED} the viscoelastic deflection of an infinite floating ice plate subjected to a circular load, assuming the Maxwell-Voigt type four-element model. We developed^{WAS DEVELOPED} an effective method of numerical integration of the solution integrals, of which each integrand contains a product of Bessel functions extending to infinity. We fitted^{WAS FITTED} the theoretical curve to the field data, but the material constants thus found varied with time and location.</p>		

DD FORM 1 JAN 73 1473

EDITION OF 1 NOV 65 IS OBSOLETE

Unclassified

SECURITY CLASSIFICATION OF THIS PAGE (When Data Entered)

PREFACE

This report was prepared by Dr. Shunsuke Takagi, Research Physical Scientist, Physical Sciences Branch, Research Division, U.S. Army Cold Regions Research and Engineering Laboratory.

The study was funded under DA Project 4A161102AT24, *Research in Snow, Ice and Frozen Ground*; Task A1, *Properties of Cold Regions Materials*; Work Unit 001, *Properties of Snow and Ice*. The numerical computation was partly supported by the Ice Engineering Program, CRREL.

The report was technically reviewed by Dr. D.E. Nevel, G. Frankenstein, and Dr. A. Assur of CRREL.

ACCESSION for	
NTIS	White Section <input checked="" type="checkbox"/>
DCC	Buff Section <input type="checkbox"/>
UNANNOUNCED	<input type="checkbox"/>
JUSTIFICATION.....	
.....	
DISTRIBUTION/AVAILABILITY CODES	
Dist.	ALL and/or SPECIAL
A	

CONTENTS

	Page
Abstract	i
Preface	ii
Introduction	1
1. The problem	2
2. The solution	4
3. Method of numerical integration	7
4. Ramp/steady loading	8
5. Curve fitting to time lapse deflections	10
6. Asymptotic deflection	14
7. Deflection profiles	16
Acknowledgement	17
Literature cited	18
Appendix I. Analytical background	19
Appendix II. Computer programs, ramp time profiles and steady time profiles	25

ILLUSTRATIONS

Figure	
1. Maxwell-Voigt type four element model	1
2. Definition of the ramp/steady loading	9
3. Distributed load test by Frankenstein	11
4. Concentrated load test by Frankenstein	11
5. Comparison of the calculated curves and measured points of Frankenstein's concentrated load test	12
6. Elements of TE	13
7. The TE of Frankenstein's distributed load test	13
8. The TE of Frankenstein's concentrated load test	14
9. Graphs of asymptotic integral K in (6.4)	15
10. Deflection profile	16
11. Asymptotic deflection profile	17
12. Contour of integrations (B.5) and (B.6)	20

TABLES

Table	
I. Material constants found by using the time-lapse curves of Frankenstein's distributed load test	12
II. Material constants found by using the time-lapse curves of Frankenstein's concentrated load test	12
III. Final time of the three tests	16

THE VISCOELASTIC DEFLECTION OF AN INFINITE FLOATING ICE PLATE SUBJECTED TO A CIRCULAR LOAD

Shunsuke Takagi

INTRODUCTION

Since ancient times floating ice plates have been used to cross rivers and lakes. During recent years traffic load on frozen rivers and lakes has greatly increased, and at the same time vehicles have become heavier. Aircraft landing and parking facilities also have added loads on these bodies of water. In addition, during the past several years, oil companies have started to use ice plates as drilling platforms. Thus, we now need to acquire a more detailed understanding of the creep of ice plates.

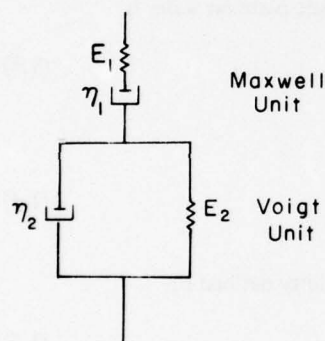


Figure 1. Maxwell-Voigt type four element model.

Formulation of the creep of a floating ice plate began after World War II with the intense development of the linear viscoelasticity theory. In 1947 Golushkevich (referred to by Kheysin¹⁰) presented an analysis assuming that ice behaves elastically for volumetric deformations and viscoelastically for deviatoric deformations. Kheysin¹⁰ used a general viscoelastic thin-plate theory to analyze the infinite floating ice plate. He used the Maxwell unit (Fig. 1) only, and considered only a concentrated load. Nevel¹¹ also used the Maxwell unit only, but considered a distributed load. He limited his numerical computation only to the center of the load.

William L. Ko, as reported by Garbaccio,^{4, 5} used the Maxwell-Voigt type four-element model (Fig. 1), which is known to represent the creep of ice satisfactorily (Jellinek and Brill⁶). In addition to thin-plate theory, Ko used Reissner's plate theory, which includes the deflection due to vertical shear forces. Garbaccio⁵ numerically evaluated Ko's solution for specific values of material constants rather

than for nondimensional parameters. Garbaccio's numerical answers show that the discontinuity of the load distribution yields a strong influence on the values of deflection. It is reasonable to suspect that his numerical evaluation may contain some errors.

IAkunin^{6, 7} has solved the same problem as Ko, but he used only thin-plate theory. Unfortunately, only an abstract of IAkunin's work is available to western researchers.

Katona⁹ and Vaudrey and Katona¹⁷ solved the same problem with a finite-element viscoelastic computer program.

We solved this problem analytically by use of thin plate theory, and also developed an effective method of numerical integration of the solution integrals. However, the theoretical curves did not satisfactorily fit the field-test curves. It is now evident that a large scale laboratory test eliminating the variation due to natural conditions must be carried out and the theoretical assumptions must be tested.

1. THE PROBLEM

We shall consider the viscoelastic ice plate floating on water extending horizontally to infinity. We shall use the Maxwell-Voigt type four-element model (Fig. 1) to describe the viscoelastic deformation of ice.

Using the notation of Fig. 1, we can show that this model gives the stress-strain relationship which we show in an operator form,

$$\epsilon = \left[\frac{1}{E_1} + \frac{1}{\eta_1 \frac{\partial}{\partial t}} + \frac{1}{E_2 + \eta_2 \frac{\partial}{\partial t}} \right] \sigma \quad (1.1)$$

where t is time. To extend the one-dimensional relationship (1.1) to the three-dimensional relationship, we assume, as explained by Flügge,² that ϵ and σ are deviatoric and relate them by

$$\sigma = 2G\epsilon$$

where G is the rigidity modulus relative to the three-dimensional deformation. Using (1.1), $2G$ is given as an operator

$$\frac{1}{2G} = \frac{1}{E_1} + \frac{1}{\eta_1 \frac{\partial}{\partial t}} + \frac{1}{E_2 + \eta_2 \frac{\partial}{\partial t}} \quad (1.2)$$

The differential equation describing the deflection w of an elastic plate on water is

$$D\nabla^4 w + \rho w = q \quad (1.3)$$

where ∇^4 is the biharmonic operator

$$\nabla^4 = \left(\frac{\partial^2}{\partial x^2} + \frac{\partial^2}{\partial y^2} \right)^2 \quad (1.4)$$

ρ the density of water, q the load per unit area, D the flexural rigidity defined by

$$D = 2Gh^3/[12(1-\nu)] \quad (1.5)$$

in which h is the thickness of the ice plate, and ν Poisson's ratio. Substituting $2G$ from (1.2) into (1.5), and D thus found into (1.3), we find the differential equation governing the viscoelastic deflection of a floating ice plate. We shall show this equation later in the nondimensional form.

We assume the load q to be a step loading applied at $t = 0$ and distributed uniformly over a circle of radius a with the center at origin. Then, letting r be the radial distance from origin

$$\begin{aligned} q &= q_0 U(t) & \text{for } 0 \leq r < a \\ &= 0 & \text{for } a < r \end{aligned} \quad (1.6)$$

where $U(t)$ is the step function, and t the time. Our problem is axisymmetric, and the biharmonic operator ∇^4 reduces to

$$\nabla^4 = \left(\frac{\partial^2}{\partial r^2} + \frac{1}{r} \frac{\partial}{\partial r} \right)^2$$

We shall nondimensionalize our differential equation. We define the characteristic length ℓ by

$$\ell^4 = E_0 h^3 / [12\rho(1 - \nu)] \quad (1.7)$$

where

$$\frac{1}{E_0} = \frac{1}{E_1} + \frac{1}{E_2}. \quad (1.8)$$

We have chosen E_0 , rather than E_1 or E_2 , to define ℓ , because E_0 is related to the secondary creep (Nevel¹²), which is the main interest in our field observation.

Let D_1 be defined by

$$D_1 = D / (\rho \ell^4). \quad (1.9)$$

Use of (1.4) and (1.7) changes (1.9) to

$$D_1 = 2G/E_0. \quad (1.10)$$

Substituting G in (1.2), (1.10) becomes

$$D_1 = 1 \left/ \left\{ \frac{E_0}{E_1} + \frac{E_0}{\eta_1 \frac{\partial}{\partial r}} + \frac{E_0}{E_2 + \eta_2 \frac{\partial}{\partial r}} \right\} \right. \quad (1.11)$$

We choose nondimensional time T

$$T = E_0 t / \eta_1 \quad (1.12)$$

and a parameter τ

$$\tau = \eta_1 E_2 / (\eta_2 E_0). \quad (1.13)$$

Then (1.11) becomes

$$D_1 = 1 \left/ \left\{ E + \frac{1}{\frac{\partial}{\partial T}} + \frac{\eta_1 / \eta_2}{\tau + \frac{\partial}{\partial T}} \right\} \right. \quad (1.14)$$

where

$$E = E_0 / E_1. \quad (1.15)$$

It is noted that

$$0 \leq E \leq 1. \quad (1.16)$$

Clearing the denominator, (1.14) becomes

$$D_1 = \frac{\partial}{\partial T} \left(\frac{\partial}{\partial T} + \tau \right) \left/ \left\{ E \frac{\partial^2}{\partial T^2} + (1 + \tau) \frac{\partial}{\partial T} + \tau \right\} \right. \quad (1.17)$$

where use is made of the relation

$$E\tau + \eta_1/\eta_2 = \tau$$

which can be proved by use of (1.13), (1.15), and (1.8).

We define the nondimensional length R by

$$R = r/\ell. \quad (1.18)$$

We replace D in (1.3) with D in (1.9), and (1.3) becomes

$$D_1 \nabla_R^4 w + w = q/\rho \quad (1.19)$$

where

$$\nabla_R^4 = \left(\frac{d^2}{dR^2} + \frac{1}{R} \frac{d}{dR} \right)^2. \quad (1.20)$$

With D_1 given by (1.17), (1.19) is the differential equation to be solved.

2. THE SOLUTION

We denote the Hankel transform of $f(R)$ by $\tilde{f}(\beta)$

$$\tilde{f}(\beta) = \int_0^\infty f(R) J_0(\beta R) R dR \quad (2.1)$$

and the two-sided Laplace transform (Van der Pol and Bremmer¹⁶) of $g(T)$ by $\bar{g}(s)$

$$\bar{g}(s) = S \int_{-\infty}^\infty g(T) e^{-sT} dT. \quad (2.2)$$

We denote the inverse of (2.2) by

$$g(T) = L^{-1} [\bar{g}(S)]. \quad (2.3)$$

Applying these two transforms, (1.19) becomes

$$\bar{D}_1 \beta^4 \tilde{w} + \tilde{w} = \tilde{q}/\rho$$

where

$$\bar{D}_1 = \frac{S(S+\tau)}{ES^2 + (1+\tau)S + \tau}. \quad (2.4)$$

Applying the two transforms to q defined by (1.6), we get

$$(1/\rho) \tilde{q} = [P/(\pi A \rho \ell^2)] (1/\beta) J_1(\beta A) \quad (2.5)$$

where

$$P = \pi a^2 q \quad (2.6)$$

and

$$A = a/\ell. \quad (2.7)$$

Thus the transformed solution is given by

$$\tilde{w} = \frac{P}{\pi A \rho \ell^2} \frac{1}{\beta(1 + \bar{D}_1 \beta^4)} J_1(\beta A).$$

Performing the Hankel inverse, we find

$$\bar{w} = \frac{P}{\pi A \rho \ell^2} \int_0^\infty \frac{1}{1 + \bar{D}_1 \beta^4} J_1(\beta A) J_0(\beta R) d\beta. \quad (2.8)$$

Performing the Laplace inverse, we find

$$w = \frac{P}{\pi A \rho \ell^2} \int_0^\infty L^{-1}\left(\frac{1}{1 + \bar{D}_1 \beta^4}\right) J_1(\beta A) J_0(\beta R) d\beta. \quad (2.9)$$

To find $L^{-1}[1/(1 + \bar{D}_1 \beta^4)]$, we compute the partial fraction

$$\frac{1}{S} \frac{1}{1 + \bar{D}_1 \beta^4} = \frac{1}{S} + \frac{\beta^4 (\tau - \alpha_2)}{\sqrt{DESC}} \frac{1}{S + \alpha_2} - \frac{\beta^4 (\tau - \alpha_1)}{\sqrt{DESC}} \frac{1}{S + \alpha_1}$$

where $-\alpha_1$ and $-\alpha_2$ are the roots of the quadratic equation

$$(E + \beta^4) S^2 + (\tau \beta^4 + 1 + \tau) S + \tau = 0. \quad (2.10)$$

They are given by

$$\left. \begin{array}{l} \alpha_1 \\ \alpha_2 \end{array} \right\} = \frac{\tau \beta^4 + 1 + \tau \mp \sqrt{DESC}}{2(\beta^4 + E)} \quad (2.11)$$

where

$$DESC = (\tau \beta^4 + 1 + \tau)^2 - 4\tau(\beta^4 + E) \quad (2.12)$$

which transforms to

$$= [\tau(\beta^4 + 1) - 1]^2 + 4\tau(1 - E). \quad (2.13)$$

From (2.13), it is clear that

$$DESC > 0. \quad (2.14)$$

The roots α_1 and α_2 are therefore always real. Moreover, inspection of (2.11) and (2.12) shows that both α_1 and α_2 are always positive. Thus we find that

$$L^{-1}\left(\frac{1}{1+\bar{D}_1\beta^4}\right) = 1 + \frac{\beta^4(\tau-\alpha_2)}{\sqrt{DESC}} e^{-\alpha_2\tau} - \frac{\beta^4(\tau-\alpha_1)}{\sqrt{DESC}} e^{-\alpha_1\tau}. \quad (2.15)$$

Substituting (2.15) into (2.9), the solution for w is found:

$$w = \frac{P}{\pi A \rho \ell^2} \int_0^\infty \left\{ 1 + \frac{\beta^4(\tau-\alpha_2)}{\sqrt{DESC}} e^{-\alpha_2\tau} - \frac{\beta^4(\tau-\alpha_1)}{\sqrt{DESC}} e^{-\alpha_1\tau} \right\} J_1(\beta A) J_0(\beta R) d\beta. \quad (2.16)$$

The radial and hoop stresses are given by

$$\sigma_r = -\frac{6D}{h^2} \left(\frac{\partial^2 w}{\partial r^2} + \frac{\nu}{r} \frac{\partial w}{\partial r} \right)$$

$$\sigma_\theta = -\frac{6D}{h^2} \left(\frac{1}{r} \frac{\partial w}{\partial r} + \nu \frac{\partial^2 w}{\partial r^2} \right)$$

respectively. Changing D to D_1 by use of (1.9) and r to nondimensional R by use of (1.18), they become

$$\sigma_r = -\frac{6\rho\ell^2}{h^2} D_1 \left(\frac{\partial^2 w}{\partial R^2} + \frac{\nu}{R} \frac{\partial w}{\partial R} \right)$$

$$\sigma_\theta = -\frac{6\rho\ell^2}{h^2} D_1 \left(\frac{1}{R} \frac{\partial w}{\partial R} + \nu \frac{\partial^2 w}{\partial R^2} \right)$$

where D_1 is the operator on T given by (1.17). The two-sided Laplace transform yields

$$\bar{\sigma}_r = -\frac{6\rho\ell^2}{h^2} \left(\frac{\partial^2}{\partial R^2} + \frac{\nu}{R} \frac{\partial}{\partial R} \right) \bar{D}_1 w \quad (2.17)$$

$$\bar{\sigma}_\theta = -\frac{6\rho\ell^2}{h^2} \left(\frac{1}{R} \frac{\partial}{\partial R} + \nu \frac{\partial^2}{\partial R^2} \right) \bar{D}_1 w \quad (2.18)$$

where $\bar{D}_1 w$ is the Laplace transform of $D_1 w$.

Using (2.8) one gets

$$\bar{D}_1 w = \frac{P}{\pi A \rho \ell^2} \int_0^\infty \frac{\bar{D}_1}{1+\bar{D}_1\beta^4} J_1(\beta A) J_0(\beta R) d\beta.$$

The Laplace inverse of this is

$$D_1 w = \frac{P}{\pi A \rho \ell^2} \int_0^\infty L^{-1} \left(\frac{\bar{D}_1}{1+\bar{D}_1\beta^4} \right) J_1(\beta A) J_0(\beta R) d\beta.$$

To find $L^{-1}[\bar{D}_1/(1+\bar{D}_1\beta^4)]$, we compute the partial fraction,

$$\frac{1}{s} \frac{\bar{D}_1}{1 + \bar{D}_1 \beta^4} = \frac{\tau - \alpha_1}{\sqrt{DESC}} \frac{1}{s + \alpha_1} - \frac{\tau - \alpha_2}{\sqrt{DESC}} \frac{1}{s + \alpha_2}.$$

Thus we find

$$L^{-1} \left(\frac{\bar{D}_1}{1 + \bar{D}_1 \beta^4} \right) = \frac{\tau - \alpha_1}{\sqrt{DESC}} e^{-\alpha_1 T} - \frac{\tau - \alpha_2}{\sqrt{DESC}} e^{-\alpha_2 T}.$$

Thus the inverse of (2.17) is

$$\sigma_r = \frac{6P}{\pi A h^2} \int_0^\infty J_1(\beta A) \left\{ J_0(\beta R) - \frac{1-\nu}{\beta R} J_1(\beta R) \right\} \frac{(\tau - \alpha_1) e^{-\alpha_1 T} - (\tau - \alpha_2) e^{-\alpha_2 T}}{\sqrt{DESC}} \beta^2 d\beta. \quad (2.19)$$

The inverse of (2.18) is

$$\sigma_\theta = \frac{6P}{\pi A h^2} \int_0^\infty J_1(\beta A) \left\{ \nu J_0(\beta R) + \frac{1-\nu}{\beta R} J_1(\beta R) \right\} \frac{(\tau - \alpha_1) e^{-\alpha_1 T} - (\tau - \alpha_2) e^{-\alpha_2 T}}{\sqrt{DESC}} \beta^2 d\beta. \quad (2.20)$$

Tabulation of σ_r and σ_θ becomes easier if linear combinations of (2.19) and (2.20) that do not contain ν are computed.

3. METHOD OF NUMERICAL INTEGRATION

It is impossible to analytically integrate the solution integrals (2.16), (2.19) and (2.20). (See App. 1.)

The direct numerical integration is inconvenient because of the slow convergence of the Bessel functions for large values of the independent variable β . We shall choose finite ranges of integration that give sufficiently close approximations. The essence of our method consists of the following integration procedure:

Consider the integral

$$I = \int_0^\infty \phi(\beta) J_1(\beta A) J_0(\beta R) d\beta \quad (3.1)$$

where the non-Bessel factor $\phi(\beta)$ is finite in the range of integration, and asymptotically

$$\phi(\beta) \sim a\beta^{-n} \quad (3.2)$$

in which a is constant. The value of n in our formulas in the previous section is ≥ 4 . The general case is discussed in Appendix 1.

We will replace the infinite integral (3.1) with a finite integral. Given a large value N , we can estimate an upper bound of the absolute integral,

$$\int_N^\infty |\phi(\beta) J_1(\beta A) J_0(\beta R)| d\beta \quad (3.3)$$

called the absolute remainder, by substituting the asymptotic expansions of $\phi(\beta)$ and Bessel functions. We let the trigonometric functions in the latter equal one. Denoting the absolute remainder by $[Abs I]_N^\infty$, we find

$$[Abs I]_N^\infty < [2a/(\pi\sqrt{aA})] (nN^n)^{-1}. \quad (3.4)$$

Let ϵ be the error we can tolerate in our computation. In our actual computation, we chose

$$\epsilon = 10^{-5}.$$

The value of N is evaluated by equating the right hand side of (3.4) to ϵ :

$$[2a/(\pi\sqrt{aA})] (nN^n)^{-1} = \epsilon. \quad (3.5)$$

Then, integral I in (3.1) is approximated by

$$I \doteq \int_0^N \phi(\beta) J_1(\beta A) J_0(\beta R) d\beta. \quad (3.6)$$

The value of N was small in most of our computation [$N \leq 10$ except in (6.4)], and our numerical scheme worked very effectively.

We list in the following the asymptotic expansions of the non-Bessel factors $\phi(\beta)$ contained in the integrands of our integral solutions (2.16), (2.19), and (2.20):

$$\begin{aligned} \alpha_1 &\sim \beta^{-4} \\ \alpha_2 &\sim \tau(1 + \beta^{-4}) \\ e^{-\alpha_1 T} &\sim 1 - T\beta^{-4} \\ e^{-\alpha_2 T} &\sim e^{-\tau T} \\ (\tau - \alpha_1)/\sqrt{DESC} &\sim \beta^{-4} - \beta^{-8} \\ (\tau - \alpha_2)/\sqrt{DESC} &\sim -(1 - E)\beta^{-8}. \end{aligned} \quad (3.7)$$

4. RAMP/STEADY LOADING

We used two load tests to fit our theoretical curves. One was the Sun Oil Corporation's (SUNOCO) data obtained during the winters of 1973-1974 and 1974-1975 at Resolute Bay, Northwest Territory (unpublished). The other was Frankenstein's data³ obtained on Portage Lake, Michigan, and the Garrison Dam Reservoir, North Dakota, on 20 March 1956 and 18 January 1957. Among these tests, we chose the ideal ramp/steady loading for our numerical computation. In this loading, as illustrated in Figure 2, the load P is increased initially at a constant rate \dot{P} and, after a certain time T_0 , kept constant at $P = \dot{P}T_0$. However, since SUNOCO does not allow the publication of their data, we cannot include their data in this paper.

We will derive the ramp/steady formulas by use of the step-loading formulas given in the previous section. However, since both SUNOCO and Frankenstein measured only deflection, we derive only the deflection formulas.

Define the influence function $w_0(T)$ by letting $P = 1$ in (2.16):

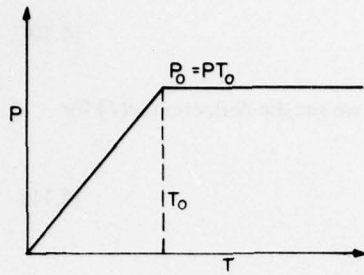


Figure 2. Definition of the ramp/steady loading.

$$w_0(T) = \frac{1}{\pi A \rho l^2} \int_0^{\infty} \left[1 + \frac{\beta^4 (\tau - \alpha_2)}{\sqrt{DESC}} e^{-\alpha_2 \tau} - \frac{\beta^4 (\tau - \alpha_1)}{\sqrt{DESC}} e^{-\alpha_1 \tau} \right] J_1(\beta A) J_0(\beta R) d\beta. \quad (4.1)$$

The deflection $w(T)$ for $0 \leq T \leq T_0$ is given by

$$w(T) = \int_0^T w_0(T - \lambda) \dot{P} d\lambda \quad (4.2)$$

and for $T_0 \leq T$ by

$$= \int_0^{T_0} w_0(T - \lambda) \dot{P} d\lambda \quad (4.3)$$

where $\dot{P} = P/T_0$.

Substituting (4.1) into (4.2) and integrating with regard to λ , we get the deflection $w(T)$ for $0 \leq T \leq T_0$:

$$w(T) = [\dot{P}/(\pi A \rho l^2)] (U_1 - U_2 + U_3) \quad (4.4)$$

where

$$U_1 = \int_0^N \frac{1}{\alpha_1} (e^{-\alpha_1 T} - 1 + \alpha_1 T) J_1(\beta A) J_0(\beta R) d\beta \quad (4.5)$$

$$U_2 = \int_0^N \left[\frac{\beta^4 (\tau - \alpha_1)}{\sqrt{DESC}} - 1 \right] \frac{1}{\alpha_1} (1 - e^{-\alpha_1 T}) J_1(\beta A) J_0(\beta R) d\beta \quad (4.6)$$

$$U_3 = \int_0^N \frac{\beta^4 (\tau - \alpha_2)}{\sqrt{DESC}} \frac{1}{\alpha_2} (1 - e^{-\alpha_2 T}) J_1(\beta A) J_0(\beta R) d\beta. \quad (4.7)$$

The absolute remainders are as follows:

$$[Abs U_1]_N^{\infty} < [T^2/(4\pi\sqrt{AR})] N^{-4} \quad (4.8)$$

$$[Abs U_2]_N^{\infty} < [T/(2\pi\sqrt{AR})] N^{-4} \quad (4.9)$$

$$[Abs U_3]_N^\infty < [(1-E)/(2\pi\sqrt{AR})] \frac{1}{T} (1 - e^{-T}) N^{-4}. \quad (4.10)$$

Substituting (4.1) into (4.3) and integrating with regard to λ , we get the deflection $w(T)$ for $T_0 \leq T$:

$$w(T) = [P/(\pi A \rho l^2)] (I_1 + I_2 + I_3) \quad (4.11)$$

where

$$I_1 = \int_0^N \left\{ 1 - \frac{\beta^4 (\tau - \alpha_1)}{\sqrt{DESC}} \frac{1}{\alpha_1 T_0} (e^{\alpha_1 T_0} - 1) \right\} J_1(\beta A) J_0(\beta R) d\beta \quad (4.12)$$

$$I_2 = \int_0^N \frac{\beta^4 (\tau - \alpha_2)}{\sqrt{DESC}} (1 - e^{-\alpha_1 T}) \frac{1}{\alpha_1 T_0} (e^{\alpha_1 T_0} - 1) J_1(\beta A) J_0(\beta R) d\beta \quad (4.13)$$

$$I_3 = \int_0^N \frac{\beta^4 (\tau - \alpha_2)}{\sqrt{DESC}} e^{-\alpha_2 T} \frac{1}{\alpha_2 T_0} (e^{\alpha_2 T_0} - 1) J_1(\beta A) J_0(\beta R) d\beta. \quad (4.14)$$

The absolute remainders are as follows:

$$[Abs I_1]_N^\infty < (2\pi\sqrt{AR})^{-1} N^{-4} \quad (4.15)$$

$$[Abs I_2]_N^\infty < [T/(2\pi\sqrt{AR})] N^{-4} \quad (4.16)$$

$$[Abs I_3]_N^\infty < [(1-E)/(2\pi\sqrt{AR})] \{ (e^{\tau T_0} - 1)/(\tau T_0) \} e^{-\tau T} N^{-4}. \quad (4.17)$$

Computer programs for these formulas are shown in Appendix II.

5. CURVE FITTING TO TIME LAPSE DEFLECTIONS

Frankenstein³ placed a 12-ft-diameter tank on the ice and pumped the adjoining water into the tank. (We call this the distributed load test.) However, the temperature of the water in the tank obviously disturbed the ice temperature. He then tried a variation by placing a 17.3-in.-diameter concrete block under the 12-ft-diameter tank. (We call this the concentrated load test.) The water in the tank was, in this case, isolated from the ice and did not disturb the ice temperature.

The load-vs-time curves of these tests and the measured deflections are shown in Figures 3 and 4. "TANK" designates the deflection of the edge of the tank. "RODS" are the sites where the measurements were taken. The distances of the measurement sites from the center of the load are listed in Tables I and II.

The material constants found by the curve fitting are shown in Tables I and II. They vary with the location of the measurement.

To show the significance of the material constant variation with the measurement sites, we chose the material constants determined at rod 1 of Frankenstein's concentrated-load time-lapse curve, and computed the deflections at the other measurement sites. Figure 5 shows the comparison of the computed curves and the measured data. The left and right columns show the ramp and steady portions of the deflection curves, respectively. They are designated by (r) and (s) respectively.

To express the degree of curve fitting we devised the trapezoidal error (TE). In Figure 6, a, A and b, B show two pairs of measured and computed deflections at two consecutive times t_1 and t_2 ,

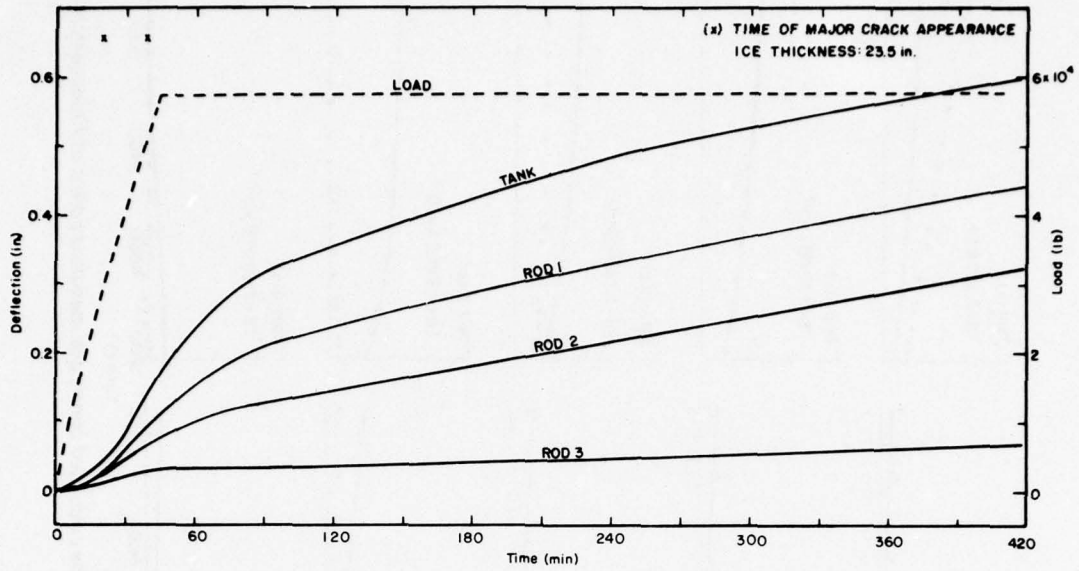


Figure 3. Distributed load test by Frankenstein (ref. 3, test 5).

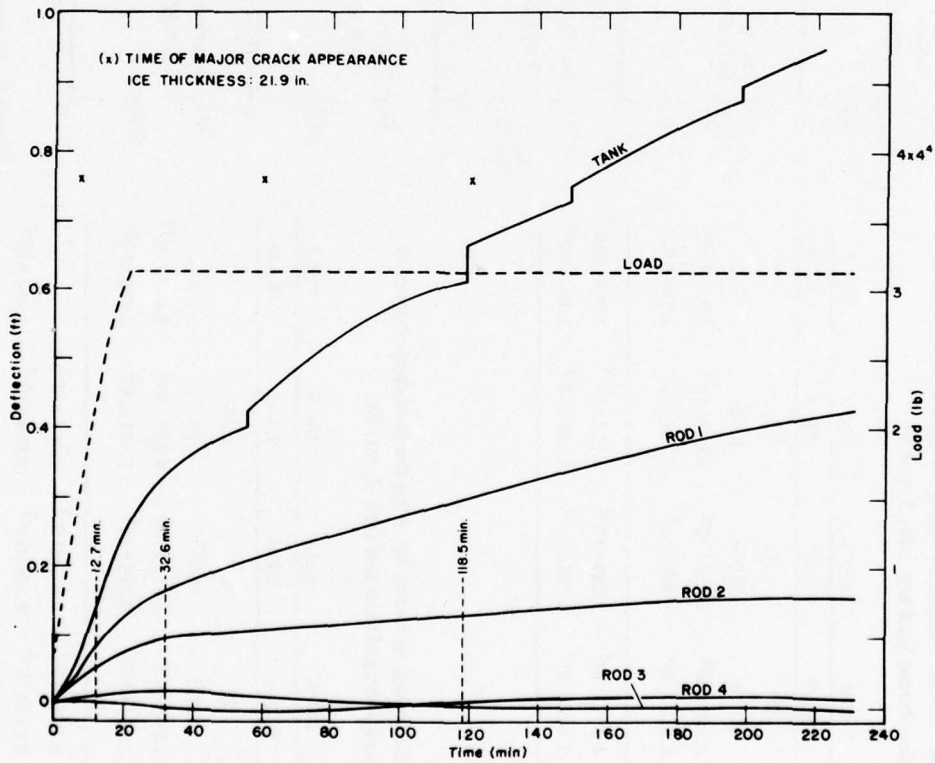


Figure 4. Concentrated load test by Frankenstein (ref. 3, test 8).

Table I. Material constants found by using the time-lapse curves of Frankenstein's distributed load test (ref. 3, test 5).

	TANK	Rod 1	Rod 2	Rod 3
Distance	1.83 m	4.9 m	9.8 m	19.6 m
τ	20	20	26	5
E	0.028	0.014	0.005	0.02
E_0 (kg/m ²)	2.159×10^8	3.729×10^8	9.812×10^8	3.925×10^9
η_1/E_0 (sec)	1.488×10^6	1.469×10^6	1.224×10^6	2.448×10^6
TE (ramp) (m)	4.928×10^{-3}	2.780×10^{-3}	3.117×10^{-3}	1.0541×10^{-3}
TE (flat) (m)	3.048×10^{-3}	2.195×10^{-3}	3.882×10^{-3}	1.393×10^{-3}

Table II. Material constants found by using the time-lapse curves of Frankenstein's concentrated load test (ref. 3, test 8).

	TANK	Rod 1	Rod 2	Rod 3
Distance	0.22 m	4.9 m	9.8 m	19.6 m
τ	2	6.5	20	5
E	0.0005	0.007	0.05	0.1
E_0 (kg/m ²)	1.766×10^6	9.813×10^7	6.869×10^8	9.813×10^{11}
η_1/E_0 (sec)	2.815×10^6	4.896×10^5	1.101×10^6	2.448×10^6
TE (ramp) (m)	4.718×10^{-3}	5.812×10^{-3}	2.063×10^{-3}	
TE (flat) (m)	4.727×10^{-3}	2.730×10^{-3}	2.884×10^{-4}	2.750×10^{-3}

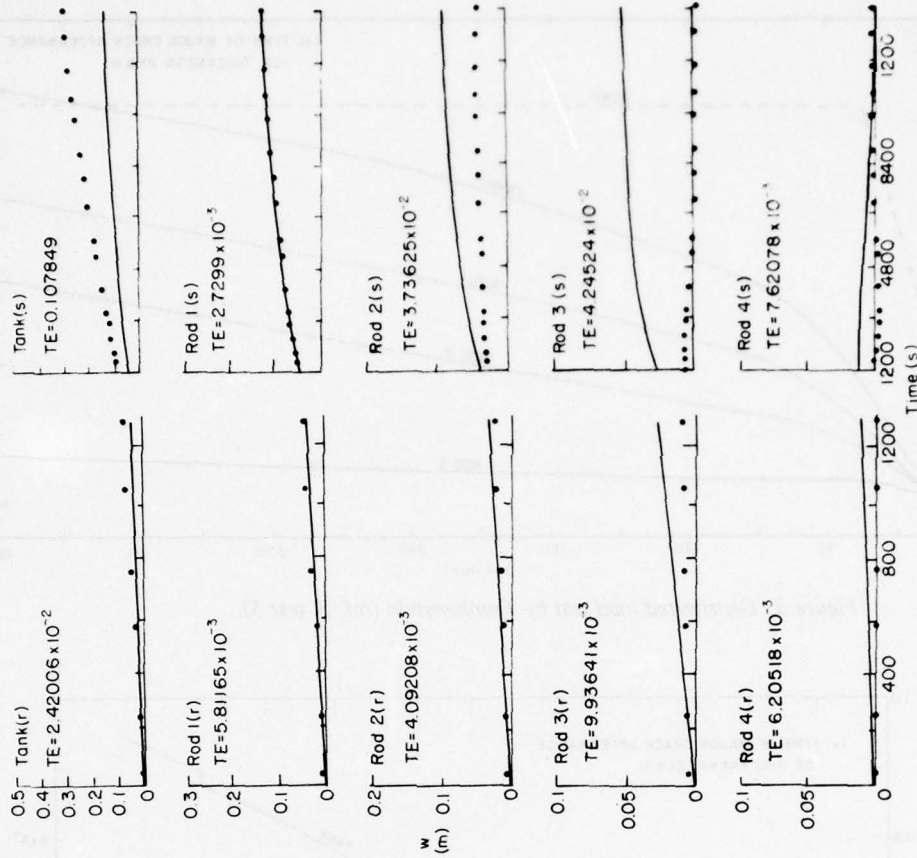


Figure 5. Comparison of the calculated curves and measured points of Frankenstein's concentrated load test.

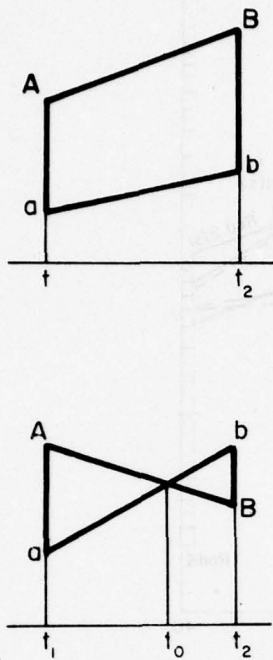


Figure 6. Elements of TE.

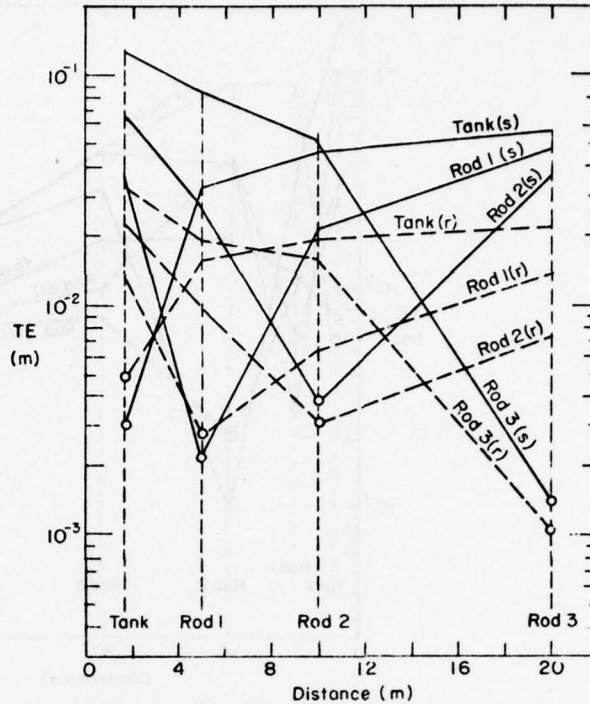


Figure 7. The TE of Frankenstein's distributed load test (ref. 3, test 5).

respectively. We squared A-a and B-b and, in case of the upper figure where the errors are of the same sign, computed the area of the trapezoid of which the bases are $(A-a)^2$ and $(B-b)^2$ and the height $t_2 - t_1$. In case of the lower figure where the errors change sign, we calculated the sum of the areas of the two triangles of which the bases are $(A-a)^2$ and $(b-B)^2$ and the heights $t_0 - t_1$ and $t_2 - t_0$ respectively, where t_0 is the abscissa of the intersection. Denoting by S the area of such a figure, we defined TE by

$$TE = \sqrt{(\sum S)/T} \quad (5.1)$$

where the summation is over all the intervals and T the sum of the abscissa intervals.

The TE indicates a sort of absolute maximum error. Its unit is m . If the deflections are of ordinary magnitude, the TE of order 10^{-3} and 10^{-2} means a good and tolerable fit, respectively. If the deflections are very small, as in the case of rod 4, the smallness of the value of TE does not mean much. We did not list the computed values at rod 4 in Tables I and II.

We evaluated the TE for all the possible cases. They are shown in Figures 7 and 8. The abscissa is the distance from the center of the load. The measurement sites are noted on the abscissa axis. The circled points are those whose material constants are used to compute a set of TE. The sets of TE thus computed are connected with solid or broken lines and labeled with the appellations of the circled measurement sites.

Comparison of Figures 7 and 8 shows that the concentrated load test has smaller overall TE values than the distributed load test. However, we cannot recognize any significant effect of the temperature distribution due to the watertank temperature disturbance. Probably the cracks, whose appearances are noted in Figures 3 and 4 but are not considered in our formulation, were more detrimental

After the numerical computation was finished in 1976, Dr. Andrew Assur, an ice mechanics expert at CRREL, notified us that the variations of material constants in Tables I and II are in the

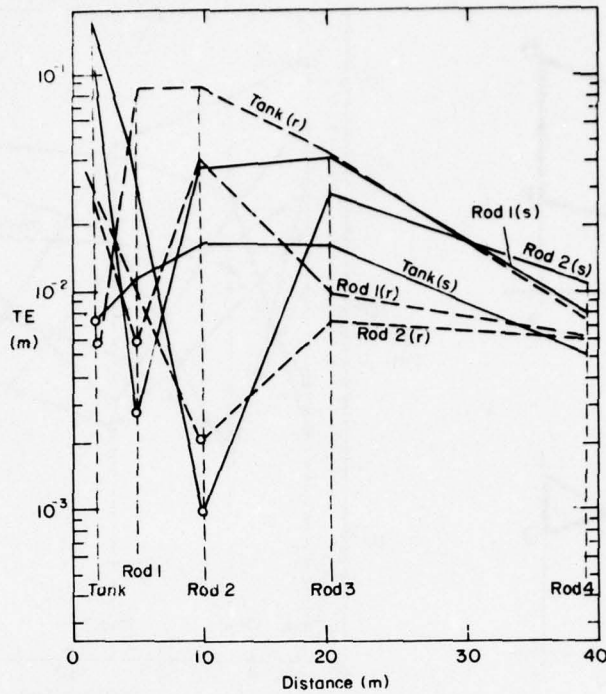


Figure 8. The TE of Frankenstein's concentrated load test (ref. 3, test 8).

range of reasonable values from the viewpoint of the nonlinear viscoelastic constants (Shumskij¹⁴). We tried in 1977 to reevaluate the material constants; we thought that, although the theoretical curve is formulated on the linear assumption, if we fit the theoretical curve in the narrow time interval and space span, we can find the material constants close to the incremental viscoelastic constants. However, this plan could not be executed because the distances between the measuring rods were too large.

6. ASYMPTOTIC DEFLECTION

We shall show in the following that only one material constant is contained in the asymptotic formulas. The curve fitting, therefore, must be carried out in the initial stage.

Referring to the asymptotic relationships in (3.7), we find that, when T is large, both the step-loading formulation (2.16) and the ramp/steady loading formulation (4.11) reduce to

$$w = [P/(\pi A \rho l^2)] (K/A) \quad (6.1)$$

where

$$\frac{1}{A} K = \int_0^{\infty} (1 - e^{-T\beta^4}) J_1(\beta A) J_0(\beta R) d\beta. \quad (6.2)$$

It is assumed in this derivation that $\tau > 0$, and that only large values of β are effective in the integration. Letting

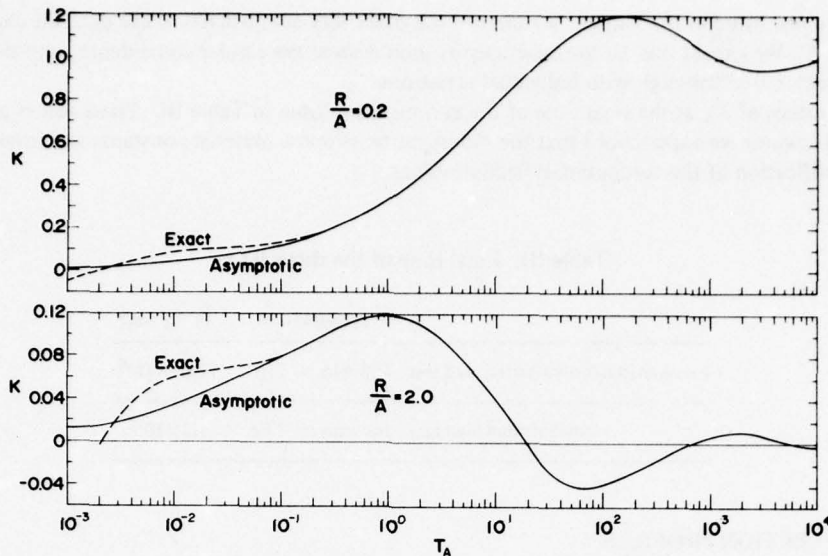


Figure 9. Graphs of asymptotic integral K in (6.4).

$$x = \beta A \quad (6.3)$$

(6.2) becomes

$$K = \int_0^{\infty} (1 - e^{-T_A x^4}) J_1(x) J_0[(R/A)x] dx \quad (6.4)$$

where

$$T_A = TA^4 \quad (6.5)$$

$$= \frac{t_0^4}{h^3} \frac{12\rho(1-\nu)}{\eta_1} \quad (6.6)$$

Thus, all the material constants are lumped into the second factor of (6.6). The stress formulas, although not mentioned here, can be similarly transformed.

As shown in Appendix I, (6.4) cannot be analytically integrated; it must be numerically integrated. To effect the numerical integration, the non-Bessel factor in (6.4) is so chosen that it becomes zero at $x = \infty$. The absolute remainder is estimated:

$$[Abs K]_{\infty}^{\infty} < \left[T_A \frac{1}{2\pi} \sqrt{\frac{A}{R}} \right] N^{-4}. \quad (6.7)$$

Graphs of integral K for the values of $R/A = 0.2$ and 2.0 are shown in Figure 9. When $T_A = \infty$, the non-Bessel factor becomes equal to one. At this limit, therefore, $K = 1$ when $R < A$, and $K = 0$ when $R > A$. As shown in the graphs, this limit is almost reached when $T_A > 1000$.

Exact integral K was formulated for the ramp/steady loading, and evaluated by use of a set of constants: $T_0 = 6 \times 10^3$ sec, $\tau = 10$, $E = 1/6$, $\eta_1/E_0 = 6.12 \times 10^4$ sec = 17 hr, $E_0 = 7 \times 10^8$ kg/m², $\nu = 0.5$, and $A = 0.5$. These constants give $l = 29.31$ m and $T_A = t(2.48 \times 10^{-3} \text{ day}^{-1})$. As shown in Figure 9, the asymptotic integral K is very close to the exact integral in the range $T_A > 0.1$. The above constants are the rough estimates used before starting the elaborate calculations.

They are not listed in the Tables. We did not use other sets of constants to evaluate the exact integral K . We expect that all the exact curves should show the similar coincidence with the asymptotic curve although with individual variations.

The values of T_A at the final time of the two tests are listed in Table III. These values are very small. However we experienced that the modification of some material constants was insensitive on the modification of the computed deflection values.

Table III. Final time of the three tests.

	in physical unit	in T_A unit
Frankenstein's distributed load test	420 min = 7 hr	2.67×10^{-4}
concentrated load test	240 min = 4 hr	1.2×10^{-8}

7. DEFLECTION PROFILES

We computed the deflection profiles of the concentrated load test (Frankenstein,³ test 8) at 12.7, 32.6, and 118.5 min by use of the material constants, $\tau = 10$, $E = 0.02$, $\eta_1/E = 7 \times 10^5$ sec, and $E_0 = 2 \times 10^8$ kg/m², as shown in Figure 10. These material constants are round numbers intermediate between the material constants at rod 1 and rod 2 in Table II. The three chosen times mentioned above are marked in Figure 4. The computed profiles are quite different from the measured profiles. We varied the material constants but could not find values that make the theoretical curve assume a similarity to the measured curve. It is our impression that the measured profiles do not belong to the family of curves that our analytical formula can describe. The measured and computed curves intersect between rod 1 and rod 2, indicating the reliability of our computation, as may be expected from the choice of the material constants.

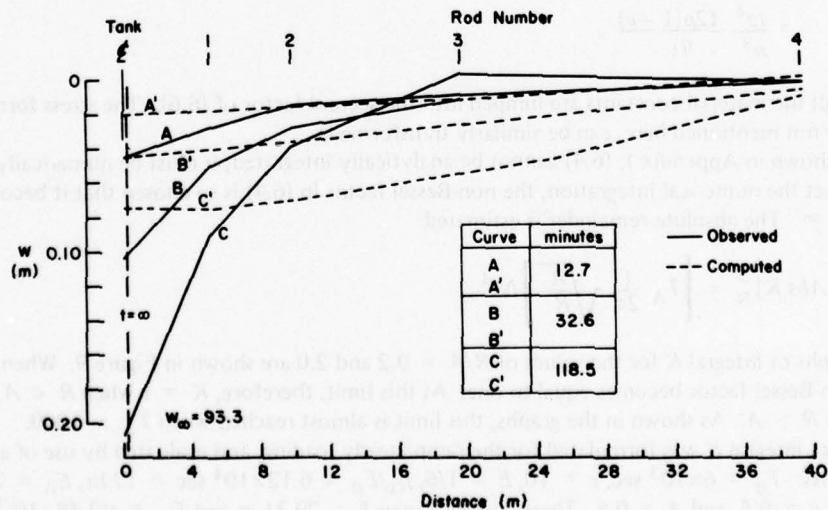


Figure 10. Deflection profile. (Frankenstein's concentrated load test, ref. 3, test 8.)

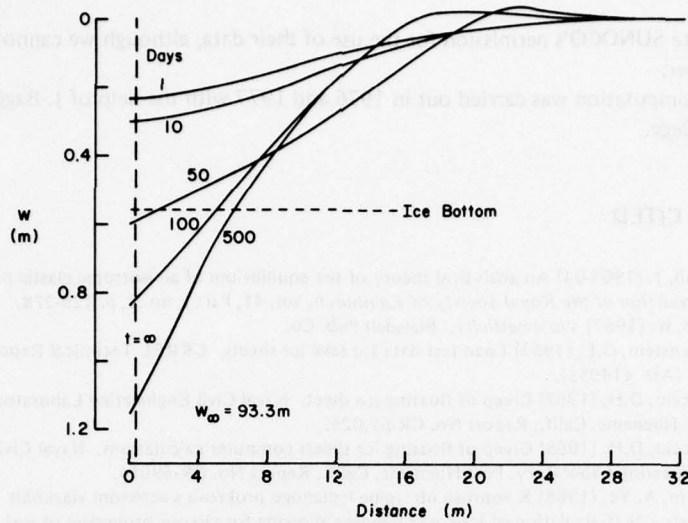


Figure 11. Asymptotic deflection profile. (Theoretical continuation of Frankenstein's concentrated load test, ref. 3, test 8.)

At $t = \infty$, the integral K in (6.4) becomes

$$\begin{aligned}
 K &= 1 && \text{for } 0 < r < a \\
 &= 0 && \text{for } 0 < a < r.
 \end{aligned}
 \tag{7.1}$$

The deflection w_∞ at $t = \infty$ is

$$\begin{aligned}
 w_\infty &= q/p && \text{for } 0 < r < a \\
 &= 0 && \text{for } 0 < a < r.
 \end{aligned}
 \tag{7.2}$$

Therefore, the water tank sinks theoretically to $w_\infty = 93.3$ m in the case of the concentrated load. However, the ice thickness h is 0.556 m. Our analytical formulas, therefore, become invalid beyond a certain elapsed time. (In the case of the distributed load test, $w_\infty = 1.350$ m and $h = 0.597$ m.)

Theoretical deflection profiles for large times are shown in Figure 11. At time infinity, our analytical deflection comes to the vertical line denoted by $t = \infty$. Because $T_A = 5.41 \times 10^{-8} \times t$ (days) in the case of the concentrated load test, the largest time, 500 days, chosen for this calculation is still too short. However, the mode of approach to the ultimate $t = \infty$ curve is observable with the curves in Figure 11. [In the case of the distributed load test, $T_A = 1.98 \times 10^{-4} \times t$ (days).]

ACKNOWLEDGEMENT

When I was struggling to understand the analytical background, Dr. D. Freitag, Technical Director, CRREL, requested Dr. Noble, Director, Mathematical Research Center, University of Wisconsin, to help me resolve some difficulties. Dr. Noble's encouragement enabled me to start the numerical integration in this paper. He later held a session for me at MRC with the participation of Drs. R.A. Askey and W. Gautschi, members of MRC, for the further clarification of the analytical background.

This research was carried out with the close cooperation of Dr. D.E. Nevel, CRREL. Especially, he contributed the nondimensional formulation of (1.19).

We appreciate SUNOCO's permission for the use of their data, although we cannot include the data in this paper.

Numerical computation was carried out in 1976 and 1977 with the help of J. Bagger, student at Dartmouth College.

LITERATURE CITED

1. Dougall, J. (1903-04) An analytical theory of the equilibrium of an isotropic elastic plate. *Transaction of the Royal Society of Edinburgh*, vol. 41, Part I, no. 8, p. 129-228.
2. Flügge, W. (1967) *Viscoelasticity*. Blaisdell Pub. Co.
3. Frankenstein, G.E. (1963) Load test data for lake ice sheets. CRREL Technical Report 89. (AD 414955).
4. Garbaccio, D.H. (1967) Creep of floating ice sheet. Naval Civil Engineering Laboratory, Port Hueneme, Calif., Report No. CR-67.025.
5. Garbaccio, D.H. (1968) Creep of floating ice sheets computer calculations. Naval Civil Engineering Laboratory, Port Hueneme, Calif., Report No. CR-69014.
6. I Akunin, A. Ye. (1968) K voprosu ob izgibe ledianogo prokrova s uchedom viazkokh svolstv l'da (Calculation of ice-cover bending allowing for viscous properties of ice). *Transactions, Novosibirskiy Institut Inzhenerov Zheleznodoroznogo Transporta*, vol. 79, p. 79-82. (Available as CRREL Draft Translation 425).
7. I Akunin, A. Ye (1970) Issledovaniye vliyaniya vremeni deystviya nagruzki na nesushchuyu sposobnost' ledyanogo pokrova (The investigation of the effect of the loading time on the bearing capacity of an ice cover). Novosibirskiy Institut Inzhenerov Zheleznodoroznogo Transporta, Speciality 01.022, Resistance of Materials and Structural Mechanics, p. 1-22.
8. Jellinek, H.H.G. and R. Brill (1956) Viscoelastic properties of ice. *Journal of Applied Physics*, vol. 27, p. 1198.
9. Katona, M.G. (1974) Ice engineering: Viscoelastic finite element formulation. Naval Civil Engineering Laboratory, Port Hueneme, Calif., Technical Report R803.
10. Kheysin, D. Ye. (1964) K zadache uprugo-plasticheskogo izgiba ledyanogo pokrova (On the problem of the elastic-plastic bending of an ice cover). *Trudy Arkticheskogo i Antarkticheskogo Nauchno-Issledovatel'skogo Instituta*, Tom. 267, p. 143.
11. Nevel, D.E. (1966) Time-dependent deflection of a floating ice sheet. CRREL Research Report 196. (AD 638717).
12. Nevel, D.E. (1976) Creep theory for a floating ice sheet. CRREL Special Report 76-4. (AD A026122).
13. Nevel, D.E., Personal communication.
14. Shumskij, P.A. (1974) *Über das fließgesetz in polykristallinem Eis*. *Polarforschung*, vol. 44, no. 2, p. 105-116.
15. Titchmarsh, E.C. (1939) *The theory of functions*. Oxford University Press.
16. Van der Pol, B. and H. Bremmer (1959) *Operational calculus based on the two-sided Laplace integral*. Cambridge at the University Press.
17. Vaudry, K.D. and M.G. Katona (1975) Viscoelastic finite element analysis of sea ice sheets. International Association of Hydraulic Research, Third International Symposium on Ice Problems, CRREL.
18. Watson, G.N. (1962) *A treatise on the theory of Bessel functions*. Cambridge at the University Press.
19. Wyman, M. (1950) Deflections of an infinite water. *Canadian Journal of Research*, vol. A28, p. 293.

APPENDIX I. ANALYTICAL BACKGROUND

A. The following theorem shows the condition under which the integral (3.1) becomes either discontinuous or continuous at $R = A$.

Theorem 1. The integral (3.1) is discontinuous or continuous at $R = A$ when n in (3.2) is equal to or larger than zero, respectively.

Proof. We can rewrite (3.1) to a one-parameter integral

$$I(\alpha) = \int_0^{\infty} f(x, \alpha) dx \quad (\text{A.1})$$

by letting $x = \beta A$, i.e. $\alpha = R/A$, where $f(x, \alpha)$ is continuous with regard to x and α . The condition that $I(\alpha)$ is a continuous function of α is that the integral (A.1) converges uniformly with respect to α (c.f. Titchmarsh,¹⁵ p. 25). The integral (A.1) uniformly converges when $n > 0$, but does not when $n = 0$.

B. We shall consider in the following the integral (3.1) whose non-Bessel factor $\phi(\beta)$ is finite in the range of integration but asymptotically becomes zero in a more general form than in the specific form (3.2).

Let an asymptotic expansion of $\phi(\beta)$ be

$$\phi(\beta) \sim \sum_{n=0}^m \phi_n(\beta). \quad (\text{B.1})$$

Rewrite (3.1) as

$$I = I_0 + \sum_{n=0}^m K_n \quad (\text{B.2})$$

where

$$I_0 = \int_0^{\infty} \left\{ \phi(\beta) - \sum_{n=0}^m \phi_n(\beta) \right\} J_1(\beta A) J_0(\beta R) d\beta \quad (\text{B.3})$$

and

$$K_n = \int_0^{\infty} \phi_n(\beta) J_1(\beta A) J_0(\beta R) d\beta. \quad (\text{B.4})$$

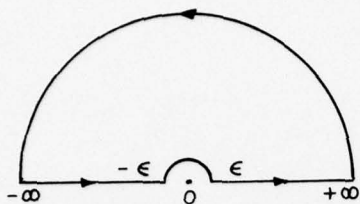


Figure 12. Contour of integrations (B.5) and (B.6).

We choose such an integer m that makes J_0 rapidly convergent. We choose such a function $\phi_n(\beta)$ that makes (B.4) analytically integrable. The following theorem is useful for the choice of $\phi_n(\beta)$.

Theorem 2. Let $F(z)$ be an even function of the complex variable $z = x + iy$ that becomes zero at $z = \infty$ and possesses only algebraic singularities (pole or branch points) on the upper half plane but no poles on the real axis. Then

$$\int_0^{\infty} F(x) J_1(ax) J_0(bx) dx$$

$$= \frac{1}{a} F(0) + \frac{1}{2} \int_{-\infty}^{+\infty} F(z) H_1^{(1)}(az) J_0(bz) dz \quad \text{when } a > b > 0 \quad (\text{B.5})$$

$$= \frac{1}{2} \int_{-\infty}^{+\infty} F(z) J_1(az) H_0^{(1)}(bz) dz \quad \text{when } 0 < a < b \quad (\text{B.6})$$

where $\int_{-\infty}^{+\infty} dz$ means the integral along the contour in Figure 12, where radius ϵ is infinitesimal, and the z -plane is cut along the negative real axis.

Proof. Consider the contour integrals

$$I(a > b) = \frac{1}{2} \int_{-\infty}^{+\infty} F(z) H_1^{(1)}(az) J_0(bz) dz \quad (\text{i})$$

where $a > b > 0$, and

$$I(a < b) = \frac{1}{2} \int_{-\infty}^{+\infty} F(z) J_1(az) H_0^{(1)}(bz) dz \quad (\text{ii})$$

when $0 < a < b$. Use of the asymptotic formulas show that $H_1^{(1)}(az) J_0(bz)$ and $J_1(az) H_0^{(1)}(bz)$ are zero on the infinitely large circle when $a > b > 0$ and $0 < a < b$, respectively. Therefore we may consider only the contour along the real axis

$$I(a > b) = \frac{1}{2} \int_{-\infty}^{+\infty} F(z) H_1^{(1)}(az) J_0(bz) dz \quad (\text{iii})$$

$$I(a < b) = \frac{1}{2} \int_{-\infty}^{+\infty} F(z) J_1(az) H_0^{(1)}(bz) dz. \quad (\text{iv})$$

We divide the real axis in three parts: $-\infty \sim -\epsilon$, $-\epsilon \sim \epsilon$, and $\epsilon \sim \infty$. We let $z = -x$ in the region $-\infty \sim -\epsilon$, and $z = x$ in the region $\epsilon \sim \infty$, neglect the infinitesimal terms, and let

$$F(z) = F(0)$$

$$H_1^{(1)}(az) = -2i/(\pi az)$$

$$H_0^{(1)}(bz) = [2i/(bz)] \log(bz/2).$$

Then (iii) and (iv) become

$$I(a > b) = -\frac{1}{a} F(0) + \int_0^\infty F(x) J_1(ax) J_0(bx) dx \quad (v)$$

$$I(a < b) = \int_0^\infty F(x) J_1(ax) J_0(bx) dx. \quad (vi)$$

Equations (v) and (vi) prove (B.5) and (B.6), respectively.

C. The need of Theorem 2 appears frequently in the mathematical study of the problems of a floating ice plate and the problems of an elastic plate on an elastic foundation. A similar integral including only one Bessel function was proved by Dougal (ref. 1, p. 138 and 147) as early as in 1903.

When $t = 0$, our solution of the viscoelastic plate reduces to the solution of the elastic plate. The elastic solution thus found is composed of the following integrals:

$$M_0 = \int_0^\infty \frac{1}{1+x^4} J_1(ax) J_0(bx) dx$$

$$M_1 = \int_0^\infty \frac{x}{1+x^4} J_1(ax) J_1(bx) dx$$

$$M_2 = \int_0^\infty \frac{x^2}{1+x^4} J_1(ax) J_0(bx) dx$$

where $a = AE^{1/4}$ and $b = RE^{1/4}$. We can carry out these integrals by direct or indirect application of Theorem 2:

$$M_0 = \text{ber } b \text{ ker}' a - \text{bei } b \text{ kei}' a + a^{-1} \quad \text{when } b \leq a$$

$$= \text{ber}' a \text{ ker } b - \text{bei}' a \text{ kei } b \quad \text{when } a \leq b$$

$$M_1 = -\text{ber}' b \text{ ker}' a + \text{bei}' b \text{ kei}' a \quad \text{when } b \leq a$$

$$= -\text{ber}' a \text{ ker}' b + \text{bei}' a \text{ kei}' b \quad \text{when } a \leq b$$

$$M_2 = \text{bei } b \text{ ker}' a + \text{ber } b \text{ kei}' a \quad \text{when } b \leq a$$

$$= \text{bei}' a \text{ ker } b + \text{ber}' a \text{ kei } b \quad \text{when } a \leq b.$$

M_0 and M_2 are found by directly applying the theorem. M_1 is found by differentiating M_0 with regard to B . Wyman¹⁹ derived M_0 by integrating a concentrated-load elastic-plate solution over the loading circle.

The continuity of M_0 and M_2 at $a = b$ is obvious on the strength of Theorem 1. We shall show, however, a direct proof in the following. We shall prove that

$$\text{ber}x \text{ker}'x - \text{beix} \text{kei}'x + x^{-1} = \text{ber}'x \text{ker}x - \text{bei}'x \text{keix} \quad (\text{C.1})$$

and

$$\text{beix} \text{ker}'x + \text{ber}x \text{kei}'x = \text{bei}'x \text{ker}x + \text{ber}'x \text{keix}. \quad (\text{C.2})$$

To prove this, note that

$$w_1(x) = \text{ber}x + i \text{beix} \quad (\text{C.3})$$

and

$$w_2(x) = \text{ker}x + i \text{keix} \quad (\text{C.4})$$

are the solutions of the differential equation

$$\frac{d^2 w}{dx^2} + \frac{1}{x} \frac{dw}{dx} - iw = 0.$$

This can be proved by decomposing the equation

$$\left(\frac{d^2}{dx^2} + \frac{1}{x} \frac{d}{dx} \right)^2 w + w = 0$$

of which (C.3) and (C.4) are the solutions.

We can find that the Wronskian

$$\begin{vmatrix} w_1(x) & w_2(x) \\ w_1'(x) & w_2'(x) \end{vmatrix}$$

is equal to

$$= -x^{-1}.$$

Thus we have the identity

$$\begin{vmatrix} \text{ber}x + i \text{beix} & \text{ker}x + i \text{keix} \\ \text{ber}'x + i \text{bei}'x & \text{ker}'x + i \text{kei}'x \end{vmatrix} = -\frac{1}{x}$$

of which the real part gives (C.1) and the imaginary part gives (C.2).

Theorem 2 can be extended in many ways. Nevel¹⁸ found that

$$\int_0^{\infty} F(x) dx = \frac{i}{\pi} \int_{-\infty}^{+\infty} F(z) \log z dz \quad (\text{C.3})$$

for an odd function $F(z)$ that does not have any pole on the real axis and vanishes at $z = \infty$.

D. It is impossible to apply Theorem 2 to the integrals of w in (2.16), σ_r in (2.19), and σ_θ in (2.20) for the following reason.

The function $\exp(-\alpha_2 T)$ has essential singularities at the roots of

$$\beta^4 + E = 0,$$

because

$$\lim_{\beta^4 \rightarrow -E} \alpha_2 = \infty$$

The function $\exp(-\alpha_1 T)$ does not possess any essential singularities because the limit of

$$\alpha_1 = 2\tau / [\tau\beta^4 + 1 + \tau + \sqrt{(\tau\beta^4 + 1 + \tau)^2 - 4\tau(\beta^4 + E)}]$$

is finite. However, the real part of α_1 becomes negative, and $\exp(-\alpha_1 T)$ diverges, as $|\beta| \rightarrow \infty$ in a certain range of direction.

Theorem 2 does not apply to integral K in (6.4) because the point $x = 0$ is an essential singularity.

The only alternative we can find for the integration of (3.1) is the use of Barnes' integral method. It consists in substituting the integrals

$$J_\nu(x) = \frac{1}{2\pi i} \int_{-\infty i}^{\infty i} \frac{\Gamma(-S)(\frac{1}{2}x)^{\nu+2S}}{\Gamma(\nu+S+1)} dS \quad (D.1)$$

$$\pi e^{\frac{1}{2}(\nu+1)\pi i} H_\nu^{(1)}(z) = \frac{1}{2\pi i} \int_{-c-\infty i}^{-c+\infty i} \Gamma(-\nu-S) \Gamma(-S) \left(-\frac{i}{2}z\right)^{\nu+2S} dS \quad (D.2)$$

for $J_\nu(x)$ and $H_\nu^{(1)}(z)$, respectively, where c is a real number satisfying $c > R(\nu)$, z is complex, and x is real. We can usually exchange the order of integration to carry out the integration with regard to x or z . Then, we can carry out the rest of the integration in most cases by use of the theorem of residue. Only the forms (D.1) and (D.2) serve this purpose. The other Barnes' representations of $J_\nu(x)$ and $H_\nu^{(1)}(z)$ do not enable us to carry out the above two procedures.

However, as mentioned by Watson (ref. 18, p. 192), (D.1) does not hold true for $\nu = 0$, and (D.2) does not hold true when $\nu = 0$ and z is real. In these two cases, the integrands of (D.1) and (D.2) become proportional to s^{-1} as s approaches $i\infty$ as the limit on the imaginary axis. Therefore we cannot use Barnes' integral method to carry out our integrals.

THIS PAGE IS BEST QUALITY PRACTICABLE FROM COPY FURNISHED TO DDC

APPENDIX II. COMPUTER PROGRAMS
Ramp Time Profiles

```

100 * NUMERICAL STUDY OF THE VISCOELASTIC DEFORMATION
110 * OF THE ICE PLATE UNDER A CIRCULAR LOAD
120 * S. TAKAHASHI, 1976 (J. BAGGER)
130 * [RAMP FORMULATION]
140
150
160
170 * .....PLOTTING OF EXPERIMENTAL DATA.....
180 * .....
190
200 * THIS SECTION OF THE PROGRAM PLOTS THE FIELD DATA FROM
210 * GUENTHER FRANKENSTEIN'S TESTS ON LAKE ICE SHEETS. THE
220 * DEFORMATION OF THE ICE FROM A CIRCULAR LOAD WAS MEASURED
230 * UNDER VARIOUS CONDITIONS. THIS DATA IS COMPARED BELOW
240 * WITH THE RAMP FORMULATION OF THE VISCOELASTIC THEORY
250 * FOR DEFORMATION.
260
270
280 * .....SYMBOL TABLE.....
290 * A DEFINED BELOW IN MAIN PROGRAM SYMBOL TABLE
300 * AY PHYSICAL LOAD RADIUS
310 * AA DATA FILE NAME
320 * E DEFINED BELOW IN MAIN PROGRAM SYMBOL TABLE
330 * EA ED -- EQUATION 1.8
340 * MY PHYSICAL ICE THICKNESS
350 * J COUNTER
360 * LY CHARACTERISTIC LENGTH
370 * MY N/ZE
380 * ND NU -- EQUATION 1.5
390 * P NON-DIMENSIONALIZED P-DOT -- EQUATION 4.3
400 * PY PHYSICAL P-DOT
410 * R DEFINED BELOW IN MAIN PROGRAM SYMBOL TABLE
420 * K5 RHO -- EQUATION 1.3
430 * KY PHYSICAL RADIUS OF OBSERVATION
440 * T DEFINED BELOW IN MAIN PROGRAM SYMBOL TABLE
450 * T1 T2 DEFINED BELOW IN MAIN PROGRAM SYMBOL TABLE
460 * T3 MAXIMUM NON-DIMENSIONALIZED T
470 * X MAXIMUM X-PLOT
480 * X5 MAXIMUM Y-PLOT
490 * Y5
500 * .....
510
520
530 * SET UP PLOTTER DETAILS
540
550 LIBRARY "PHYSLIB";FLABEL"
560 LIBRARY "PLOTLIB";TEKTO"
570 DIM C(600)
580 DIM CS(600)
590 PRINT "INPUT FILE:"
600 INPUT AS
610 FILE#1=AS
620 PRINT "RWAK";
630 INPUT AS
640 PRINT "YMAX";
650 INPUT Y5
660 CALL "PLABEL"(C),O,AS,-Y5,Y5,"TIME (SEC)",M (METERS),P=1
670 CALL "CONNECT"(C),O,O,AS,O

```

```

680
690 * INPUT TEST SITE DATA
700
710 INPUT#1: P9,H9,R9
720 * P9 = P-DOT
730 * H9 = ICE THICKNESS
740 * R9 = RADIUS
750
760 INPUT #1: AV
770 * A9 = PHYSICAL LOAD RADIUS
780
790 * PARAMETERS (VARY TO FIT)
800
810 LET I1 = 10
820 LET E = .02
830 LET N7 = 7.E+5
840 LET E8 = 4.E+8
850 * T1 = TAU
860 * E = E
870 * N7 = N1/EU
880 * E8 = EU
890
900 * CONSTANTS (STANDARD)
910
920 LET NO = 1000
930 LET NB = 45
940
950 * CONVERT TO NONDIMENSIONALIZED FORM
960
970 LET LY = (E0*H9*3)/(12*RS*(1-NB)) *CHAR, LENGTH
980 LET LY = LY*(1/4)
990 LET K = R9/L9
1000 LET A = AV/L9
1010 LET P = PY*N7
1020
1030 * PLOT DIMENSIONALIZED EXPERIMENTAL DATA
1040
1050 INPUT#1:M1
1060 FOR I = 1 TO N1
1070 * INPUT#1: T,M
1080 * CONVERT TO MKS UNITS
1090 LET T = T*60
1100 LET M = M*.3048
1110 CALL "MOVE"(C),T,M
1120 CALL "LABEL"(C),CS(I),M*,1,0,0
1130 NEXT I
1140 CALL "LIFT"(C)
1150 LET T5 = T
1160 * .....SAVE MAXIMUM TIME
1170 * .....
1180 * .....PLOTTING OF THEORETICAL CURVE.....
1190 * .....
1200
1210 * THIS SECTION OF THE PROGRAM PLOTS THE THEORETICAL
1220 * CURVE FOR COMPARISON WITH THE EXPERIMENTAL DATA.
1230
1240
1250 * .....SYMBOL TABLE.....

```


THIS PAGE IS BEST QUALITY PRACTICABLE
FROM COPY FURNISHED TO DDC

```

2420 * Y X/3, OR 3./X
2430 * *****
2440
2450 IF X >= 0 THEN 2510
2460 PRINT "FUNCTION J0(X): ARGUMENT MUST BE >= 0"
2470 PRINT "X=";X
2480 STOP
2490
2500
2510 IF X > 0 THEN 2590
2520
2530 * POLYNOMIAL APPROX, 0<X<=3.
2540 LET Y=X/3.
2550 LET J0 = 1 - .24999 97*Y^2 + .126562 08*Y^4
2560 LET J0 = J0 - .31638 66*Y^6 + .04444 79*Y^8
2570
2580 * POLYNOMIAL APPROX, X>3.
2590 LET Y=X./X
2600 LET F = F1 IN NBS BOOK
2610 LET F = .79788 456 - .00000 077*Y
2620 LET F = F - .00552 740*Y^2 + .00009 512*Y^3
2630 LET F = F + .00137 237*Y^4 - .00072 805*Y^5
2640 LET F = F + .00014 476*Y^6
2650 * T3 = THETA IN NBS BOOK
2660 LET T3 = X - .28539 816 - .04166 337*Y
2670 LET T3 = T3 - .00003 954*Y^2 + .00262 573*Y^3
2680 LET T3 = T3 - .00054 125*Y^4 - .00029 553*Y^5
2690 LET T3 = T3 + .00013 558*Y^6
2700 LET J0 = (1./SQN(X))*F*COS(T3)
2710
2720
2730 LET FNI = J0
2740 FNEW
2750
2760 DEF FNJ(X)
2770
2780 * ***FUNCTION SUBPROGRAM: J1(X)***
2790
2800 * POLYNOMIAL APPROXIMATIONS FROM:
2810 * HANDBOOK OF MATHEMATICAL FUNCTIONS,
2820 * U.S. DEPARTMENT OF COMMERCE, 1964
2830 * (9.4.4, 9.4.6)
2840
2850 * ***** SYMBOL TABLE *****
2860 * J1 J1(X) FIRST-ORDER BESSEL FUNCTION
2870 * F1 F1(X) IN NBS BOOK
2880 * T2 THETA1(X) IN NBS BOOK
2890 * X ARGUMENT
2900 * Y X/3, OR 3./X
2910 * *****
2920
2930
2940
2950 IF X >= 0 THEN 3000
2960 PRINT "FUNCTION J1(X): ARGUMENT MUST BE >= 0"
2970 PRINT "X=";X
2980 STOP
2990

```

```

3000 IF X > 0 THEN 3090
3010 * POLYNOMIAL APPROX, 0<X<=3.
3020 LET Y=X/3.
3030 LET J1 = .5 - .56249 985*Y^2 + .21093 573*Y^4
3040 LET J1 = J1 - .03954 289*Y^6 + .00443 319*Y^8
3050 LET J1 = X*J1
3060
3070
3080 * POLYNOMIAL APPROX, X>3.
3090 LET Y=X./X
3100 LET F = F1 IN NBS BOOK
3110 LET F = .79788 456 + .00000 156*Y
3120 LET F = F1 + .01659 667*Y^2 + .00017 105*Y^3
3130 LET F = F1 - .00249 511*Y^4 + .00113 653*Y^5
3140 LET F = F1 - .00020 033*Y^6
3150 * T2 = THETA1 IN NBS BOOK
3160 LET T2 = X - .235619 449 + .12499 612*Y
3170 LET T2 = T2 + .00005 650*Y^2 - .00657 879*Y^3
3180 LET T2 = T2 + .00075 348*Y^4 + .00079 824*Y^5
3190 LET T2 = T2 - .00029 166*Y^6
3200 LET J1 = (1./SQN(X))*F1*COS(T2)
3210
3220
3230 LET FNI = J1
3240 FNEW
3250 END
3260
3270 SUB "SIMP" :X1,X2,FNF,AL,AJE,R,T,T1
3280 * *** SUBPROGRAM: SIMPSON'S RULE INTEGRATION ***
3290
3300 * SIMPSON'S RULE FORMULA FROM:
3310 * NUMERICAL CALCULUS
3320 * WILLIAP WILNE, 1949
3330
3340 * ***** SYMBOL TABLE *****
3350 * A3 SIMPSON APPROXIMATION FOR PREVIOUS TRIAL
3360 * A4 SIMPSON APPROXIMATION FOR CURRENT TRIAL
3370 * FNF FUNCTION SUBPROGRAM FOR INTEGRAND
3380 * H INTERVAL WIDTH
3390 * I COUNTER
3400 * N 2*N = NUMBER OF INTERVALS
3410 * S1 PARTIAL SUM OF THE ODD TERMS
3420 * S2 PARTIAL SUM OF THE EVEN TERMS
3430 * X VARIABLE OF INTEGRATION
3440 * X2 UPPER BOUND OF INTEGRATION
3450 * X1 LOWER BOUND OF INTEGRATION
3460 * *****
3470
3480 IF X2>X1 THEN 3530
3490 PRINT "SUBPROGRAM SIMP: XMAXIMUM MUST BE > XMIN"
3500 PRINT "XMIN=";X1,"XMAX=";X2
3510
3520
3530 * INITIALIZE OLD APPROXIMATION
3540 LET A3=0
3550 * INITIALIZE TO 100 INTERVALS
3560 LET N = 50
3570 * CALCULATE INTERVAL WIDTH

```

```

3580 LET M=(X2-X1)/(2*N)
3590 * INITIALIZE PARTIAL SUMS
3600 LET S1=S2=0
3610 * CALCULATE PARTIAL SUMS
3620 LET X=X1
3630 FOR I=0 TO N
3640 LET S2=S2+FNF(A,E,R,T,I,X)
3650 LET X=X2+H
3660 NEXT I
3670 LET X=X1+H
3680 FOR I=1 TO N
3690 LET S1=S1+FNF(A,E,R,T,I,X)
3700 LET X=X2+H
3710 NEXT I
3720 * CALCULATE NEW APPROXIMATION
3730 LET A4=H*(S1+S2-FNF(A,E,R,T,I,X1)-FNF(A,E,R,T,I,X2))/3
3740
3750 IF ABS(A3-A4)<.1E-6 THEN 3850
3760
3770 * PREPARE TO TRY AGAIN
3780
3790 LET A3=A4
3800 LET S2=S1+S2
3810 LET S1=0
3820 LET N=2*N
3830 LET H=(X2-X1)/(2*N)
3840 GOTO 3670
3850 SUBEND
3860
3870 SUB "ERRUM"=N1,N2,FNU,FNV,FNW,A,E,R,T1,N7,R8,L9,P,E6,M1
3880 RESET1
3890 INPUT#1: N3
3900 INPUT#1: N3
3910 INPUT#1: T2,W2
3920 INPUT#1: T2,W2
3930 LET T2 = T2*60
3940 LET W2 = W2*.3048
3950 LET T3 = T2/N7
3960 CALL "SIMP": 0,N,FNU,U1,A,E,R,T3,T1
3970 CALL "SIMP": 0,N1,FNV,U2,A,E,R,T3,T1
3980 CALL "SIMP": 0,N2,FNW,U3,A,E,R,T3,T1
3990 LET W3 = U1 - U2 + U3
4000 LET W3 = W3/(3.14159*A*R8*L9*2/P) * COMPUTE NONDIMENSIONAL DEFORMATION
4010 LET E2 = (W3 - W2)
4020 LET T0 = 0
4030 LET S2 = 0
4040 FOR J = 1 TO N3 - 1
4050 INPUT#1: T4,W4
4060 LET T4 = T4*60
4070 LET W4 = W4*.3048
4080 LET T5 = T4/N7
4090 CALL "SIMP": 0,N,FNU,U1,A,E,R,T5,T1
4100 CALL "SIMP": 0,N1,FNV,U2,A,E,R,T5,T1
4110 CALL "SIMP": 0,N2,FNW,U3,A,E,R,T5,T1
4120 LET W5 = U1 - U2 + U3
4130 LET W5 = W5/(3.14159*A*R8*L9*2/P)
4140 LET E4 = (W5-W4)
4150 LET T6 = T4 - T2 + T6

```

THIS PAGE IS BEST QUALITY PRACTICABLE
FROM COPY FURNISHED TO DDC

Steady Time Profiles

```

100 * NUMERICAL STUDY OF THE VISCOELASTIC DEFORMATION
110 * OF THE ICE PLATE UNDER A CIRCULAR LOAD
120 * S. TAKAGI, 1976 (J. BAGGER)
130 * [RAMP FORMULATION -- STEADY STATE SOLUTION]
140
150
160 * *****
170 * *****PLOTTING OF EXPERIMENTAL DATA*****
180 * *****
190
200 * THIS SECTION OF THE PROGRAM PLOTS THE FIELD DATA
210 * GUENTHER FRANKENSTEIN'S TESTS ON LAKE ICE SHEETS. THE
220 * DEFORMATION OF THE ICE FROM A CIRCULAR LOAD WAS MEASURED
230 * UNDER VARIOUS CONDITIONS. THIS DATA IS COMPARED BELOW
240 * WITH THE STEADY-STATE FORMULATION OF THE VISCOELASTIC
250 * THEORY FOR DEFORMATION.
260
270
280 * *****SYMBOL TABLE*****
290 * A DEFINED BELOW IN MAIN PROGRAM SYMBOL TABLE
300 * AY PHYSICAL LOAD RADIUS
310 * A DATA FILE NAME
320 * C DEFINED BELOW IN MAIN PROGRAM SYMBOL TABLE
330 * E0 -- EQUATION 1-8
340 * HY PHYSICAL ICE THICKNESS
350 * J
360 * LY CHARACTERISTIC LENGTH
370 * N7/E0
380 * N0
390 * P -- EQUATION 1.5
400 * PY NON-DIMENSIONALIZED P-DOT -- EQUATION 4.3
410 * K PHYSICAL P-DOT
420 * K3 RHO -- EQUATION 1.3
430 * KY PHYSICAL RADIUS OF OBSERVATION
440 * I DEFINED BELOW IN MAIN PROGRAM SYMBOL TABLE
450 * TU TIME OF CONSTANT LOAD
460 * IT DEFINED BELOW IN MAIN PROGRAM SYMBOL TABLE
470 * IJ MAXIMUM NON-DIMENSIONALIZED T
480 * A
490 * X2 MAXIMUM X-PLOT
500 * Y2 MAXIMUM Y-PLOT
510 * *****
520
530
540 * SET UP PLOTTER DETAILS
550
560 LIBRARY "PHYSLIB";FLABEL"
570 LIBRARY "PLUTLIB";TEK10"
580 DIM C(QUU)
590 DIM C(QUU)
600 PRINT "INPUT FILE:"
610 INPUT A3
620 FILE1=C3
630 PRINT "AREA:"
640 INPUT A5
650 PRINT "YMAX:"
660 INPUT Y5
670

```

THIS PAGE IS BEST QUALITY PRACTICABLE
FROM COPY FURNISHED TO DDC

```

680 * INPUT TEST SITE DATA
690
700 INPUT #1: P9,H9,R9,TO
710 * P9 = P-DOT
720 * H9 = ICE THICKNESS
730 * R9 = RADIUS
740 * TO = TIME WHEN LOAD BECOMES CONSTANT
750
760 INPUT#1: AY
770 * AY = PHYSICAL LOAD RADIUS
780
790 * PARAMETERJ (VARY TO FIT)
800
810 LET I1 = IJ
820 LET E = -U2
830 LET N7 = /,E+5
840 LET E0 = C,E+8
850 * T1 = TAU
860 * E = E
870 * N7 = A1/EU
880 * E8 = EU
890
900 * CONSTANTS (STANDARD)
910
920 LET R0 = 1000 : 'RHO
930 LET H0 = .5 : 'NU
940
950 * CONVERT TO NONDIMENSIONALIZED FORM
960
970 LET LY = (E0*H9P3)/(12*R8*(1-N8)) 'CHAR. LENGTH
980 LET LY = LY*(1/4)
990 LET K = RY/L9
1000 LET A = AY/L9
1010 LET P = PY*N7
1020
1030 * PLOT DIMENSIONALIZED EXPERIMENTAL DATA
1040
1050 CALL "PLABEL"LC(),IC,X5,-Y5,P5,"TIME (SEC)",M (METERS)",Z
1060 CALL "CONNECT":C(),TO,X5,0
1070
1080 INPUT#1: N1
1090 FOR I = 1 TO N1
1100 INPUT#1: T,M
1110 LET I = I+60
1120 LET M = M+.3048
1130 CALL "MOVE":C(),T,M
1140 CALL "LABEL":C(),C5(),"+",I,0,0
1150 NEXT I
1160 CALL "LIFT":C()
1170 LET IS = I
1180 * *****SAVE MAXIMUM TIME*****
1190 * *****
1200 * *****PLOTTING OF THEORETICAL CURVE*****
1210 * *****
1220
1230 * THIS SECTION OF THE PROGRAM PLOTS THE THEORETICAL
1240 * CURVE FOR COMPARISON WITH THE EXPERIMENTAL DATA.
1250

```



```

3000 * US DEPARTMENT OF COMMERCE, 1964
3010 (Y4.4.5, 9.4.6)
3020
3030
3040 ***** SYMBOL TABLE *****
3050 J1 J1(X) FIRST-ORDER BESSEL FUNCTION
3060 F1 F1(X) IN NBS BOOK
3070 T1 T1(X) IN NBS BOOK
3080 X ARGUMENT
3090 Y X/3. OR 3./X
3100 *****
3110
3120
3130 IF X >= 0 THEN 3180
3140 PRINT "FUNCTION J1(X): ARGUMENT MUST BE >= 0"
3150 PRINT "A="X
3160 STOP
3170
3180 IF X > 5 THEN 3280
3190
3200 * POLYNOMIAL APPROX, 0<X<=3.
3210 LET Y=X/3.
3220 LET J1 = .5 - .56249 985*Y^2 + .21093 573*Y^4
3230 LET J1 = J1 - .03954 289*Y^6 + .00443 379*Y^8
3240 LET J1 = J1 - .00031 761*Y^10 + .00001 109*Y^10
3250 LET J1 = X*J1
3260 GOTO 3420
3270
3280 * POLYNOMIAL APPROX, X>3.
3290 LET Y=X./X
3300 * F1 = F1 IN NBS BOOK
3310 LET F1 = .79788 456 + .00000 156*Y
3320 LET F1 = F1 + .01659 667*Y^2 + .00017 105*Y^3
3330 LET F1 = F1 - .00249 511*Y^4 + .00113 653*Y^5
3340 LET F1 = F1 - .00020 033*Y^6
3350 * T1 = TETA1 IN NBS BOOK
3360 LET T2 = X - 2.35619 649 + .12499 612*Y
3370 LET T2 = T2 + .00005 650*Y^2 - .00637 879*Y^3
3380 LET T2 = T2 + .00074 348*Y^4 + .00079 824*Y^5
3390 LET T2 = T2 - .00029 166*Y^6
3400 LET J1 = (1./SQR(X))*F1*COS(T2)
3410
3420 LET F#J = J1
3430 F#END
3440 END
3450
3460 SUB "SIMP":X1,X2,F#F#A6,A,E,R,T,I0,T1
3470 * *** SUBPROGRAM: SIMPSON'S RULE INTEGRATION ***
3480
3490 * SIMPSON'S RULE FORMULA FROM:
3500 * NUMERICAL CALCULUS
3510 * WILLIAM MILNE, 1949
3520
3530 * ***** SYMBOL TABLE *****
3540 A3 SIMPSON APPROXIMATION FOR PREVIOUS TRIAL
3550 A4 SIMPSON APPROXIMATION FOR CURRENT TRIAL
3560 F#F FUNCTION SUBPROGRAM FOR INTEGRAND
3570 H INTERVAL WIDTH

```

THIS PAGE IS BEST QUALITY PRACTICABLE
FROM COPY FURNISHED TO DDC

```

2420 F#END
2430
2440 DEF F#(X)
2450
2460 * ***FUNCTION SUBPROGRAM: J0(X)***
2470
2480 * POLYNOMIAL APPROXIMATIONS FROM:
2490 * HANDBOOK OF MATHEMATICAL FUNCTIONS,
2500 * US DEPARTMENT OF COMMERCE, 1964
2510 (Y4.4.1, 9.4.3)
2520
2530 ***** SYMBOL TABLE *****
2540 J0 J0(X) ZEROth-ORDER BESSEL FUNCTION
2550 F F(X) IN NBS BOOK
2560 T1 T1(X) IN NBS BOOK
2570 X ARGUMENT
2580 Y X/3. OR 3./X
2590 *****
2600
2610
2620 IF X >= 0 THEN 2680
2630 PRINT "FUNCTION J0(X): ARGUMENT MUST BE >= 0"
2640 PRINT "A="X
2650 STOP
2660
2670 IF X > 5 THEN 2770
2680
2690 * POLYNOMIAL APPROX, 0<X<=3.
2700 LET Y=X/3.
2710 LET J0 = 1 - 2.24999 97*Y^2 + 1.26562 08*Y^4
2720 LET J0 = J0 - .31638 66*Y^6 + .04444 79*Y^8
2730 LET J0 = J0 - .00394 44*Y^10 + .00021 00*Y^10
2740 GOTO 2910
2750
2760 * POLYNOMIAL APPROX, X>3.
2770 LET Y=X./X
2780 * F = F IN NBS BOOK
2790 LET F = .79788 456 - .00000 077*Y
2800 LET F = F - .00552 740*Y^2 - .00009 512*Y^3
2810 LET F = F + .00137 237*Y^4 - .00072 805*Y^5
2820 LET F = F + .00014 476*Y^6
2830 * T1 = TETA IN NBS BOOK
2840 LET T2 = X - .78539 816 - .04166 397*Y
2850 LET T2 = T2 - .00003 954*Y^2 + .00262 573*Y^3
2860 LET T2 = T2 - .00034 125*Y^4 - .00029 353*Y^5
2870 LET T2 = T2 + .00013 558*Y^6
2880 LET J0 = (1./SQR(X))*F*COS(T2)
2890
2900
2910 LET F#J = J0
2920 F#END
2930
2940 DEF F#(X)
2950
2960 * ***FUNCTION SUBPROGRAM: J1(X)***
2970
2980 * POLYNOMIAL APPROXIMATIONS FROM:
2990 * HANDBOOK OF MATHEMATICAL FUNCTIONS,

```

```

4160 CALL "SIMP": D=N1,FNV,I2,A,E,R,I3,T0,T1
4170 CALL "SIMP": D=N2,FNV,I3,A,E,R,I3,T0,T1
4180 LET W3 = I1 + I2 + I3
4190 LET W5 = W3/(3.14159*A*R8*L9*2/P) 'COMPUTE NONDIMENSIONAL DEFORMATION
4200 LET E2 = (W3 - W2) 'INITIALIZE TIME SUM FOR NORMALIZATION
4210 LET T0 = 0
4220 LET S2 = 0
4230 FOR I = 1 TO N3 - 1
4240 INPUT#1: T4,M4
4250 LET T4 = T4+M4
4260 LET M4 = W4+.3048
4270 LET T5 = T4/N7
4280 CALL "SIMP": C=N1,FNV,I2,A,E,R,I5,T0,T1
4290 CALL "SIMP": C=N2,FNV,I3,A,E,R,I5,T0,T1
4300 LET W5 = I1 + I2 + I3
4310 LET W5 = W5/(3.14159*A*R8*L9*2/P)
4320 LET E4 = (W5 - W4)
4330 LET T6 = T4 - T2 + T6
4340 IF E4 > 0 THEN 4370
4350 LET S2 = S2 + .5*(T4 - T2)*(E2+4 + E4)/(E2+2 + E4*2)
4360 GOTO 4380
4370 LET S2 = S2 + .5*(T4 - T2)*(E4+2 + E2+2) 'INCREMENT TRAP. AREA SUM
4380 LET E2 = E4
4390 LET T2 = T4
4400 NEXT I
4410 LET E0 = S2/T6
4420 LET E0 = SQR(E0)
4430 SUBEND

```

THIS PAGE IS BEST QUALITY PRACTICABLE
FROM COPY FURNISHED TO DDC

```

3580 * I COUNTER
3590 * N 2*N = NUMBER OF INTERVALS
3600 * S1 PARTIAL SUM OF THE ODD TERMS
3610 * S2 PARTIAL SUM OF THE EVEN TERMS
3620 * X VARIABLE OF INTEGRATION
3630 * X2 UPPER BOUND OF INTEGRATION
3640 * X1 LOWER BOUND OF INTEGRATION
3650 * *****
3660 IF X2 < X1 THEN 3720
3670 PRINT "SUBPROGRAM SIMP: XMAXIMUM MUST BE > XMIN"
3680 PRINT "AFIN=";X1,"AMAX=";X2
3690 STOP
3700
3710 * INITIALIZE OLD APPROXIMATION
3720 LET A3=0
3730 * INITIALIZE TO 100 INTERVALS
3740 LET N = 50
3750 * CALCULATE INTERVAL WIDTH
3760 LET H=(X2-X1)/(C*N)
3770 * INITIALIZE PARTIAL SUMS
3780 LET S1=S2=0
3800 * CALCULATE PARTIAL SUMS
3810 LET X=X1
3820 FOR I=0 TO N
3830 LET S2=S2+FN*(A+E,R,T,I,X)
3840 LET A=X+H
3850 NEXT I
3860 LET A=X+H
3870 FOR I=1 TO N
3880 LET S1=S1+FN*(A+E,R,T,I,X)
3890 LET A=X+H
3900 NEXT I
3910 * CALCULATE NEW APPROXIMATION
3920 LET A4=(S1+S2)*2-S2-FN*(A+E,R,T,I,X1)-FN*(A+E,R,T,I,X2))/3
3930
3940 IF ABS(A3-A4) < 1.E-6 THEN 4050
3950
3960 * PREPARE TO TRY AGAIN
3970
3980 LET A3=A4
3990 LET S2=S1+S2
4000 LET S1=0
4010 LET N=2*N
4020 LET H=(X2-X1)/(C*N)
4030 GOTO 3660
4040
4050 SUBEND
4060
4070 SUB "ERROR":N1=N2,I1,FNV,FNV,A,E,R,T0,T1,N7,R8,L9,P,E0,N1
4080 RESET#1
4090 INPUT#1: N3
4100 INPUT#1: N3
4110 INPUT#1: N3
4120 INPUT#1: T2,M2
4130 LET I2 = T2+M2
4140 LET M2 = M2+.3048
4150 LET I3 = T2/N7

```